Published in final edited form as:
Urol Res. 2009 February ; 37(1): 11–17. doi:10.1007/s00240-008-0169-x.

Mechanism of formation of concentrically laminated spherules: Implication to Randall's plaque and stone formation

Fairland F. Amos[1,2], **Lijun Dai**[1,3], **Rajendra Kumar**[1,4], **Saeed R. Khan**[5], and **Laurie B. Gower**[1]

[1]Department of Materials Science and Engineering, University of Florida, P.O. Box 116400, Gainesville, FL 32611, USA

[2]Laboratory for Chemical Physics, Center for Biomolecular Materials Spectroscopy, New York University, New York, NY 10010, USA

[3]Enzo Life Sciences, Inc., 10 Executive Blvd., Farmingdale, NY 11735, USA

[4]Division of Bioengineering, Montana Tech of the University of Montana, Butte, MT 59701, USA

[5]Department of Pathology, University of Florida, Gainesville, FL 32611, USA

Abstract

We report on the formation of calcium phosphate multi-laminated spherules via a polymer-induced liquid-like precursor (PILP) process. In this non-classical crystallization route, the precipitation of liquid-like amorphous calcium phosphate (ACP) particles is promoted using anionic polypeptide additives, and these droplets coalesce to form globules that later crystallize into spherulites. During crystallization of the amorphous globules, the polymer additive, as well as the waters of hydration, is excluded ahead of the crystallization front, but some polymer becomes entrapped within diffusion-limited zones. This results in the formation of concentric laminations with layers of variable density from organic-rich inclusions. The striking resemblance of these spherules with the crystals of the Randall's plaque and other laminated stones suggests that such biological structures may form via an amorphous precursor process as well. Given the organic-rich environment present in the urinary tract, one might expect a large amount of organic materials to become entrapped within the stratified zones of a forming stone during this type of solidification and transformation process.

INTRODUCTION

The formation of minerals via an amorphous precursor phase is well documented in the field of biomineralization [1-6]. In this non-classical crystallization route, the initial precipitates can dictate the shape of the mature minerals if the amorphous phase undergoes a pseudomorphic transformation (i.e., crystals retain the shape of the prior phase), as is observed in certain calcium carbonate-based biostructures, e.g. the larval stages of the sea urchin spicules and mollusk shells [6-8], where the minerals are comprised of mostly amorphous calcium carbonate (ACC) during their early development. This amorphous phase is unstable, but is induced or stabilized by proteins [9] until it transforms into the thermodynamically stable calcite or aragonite polymorph. The presence of an amorphous precursor in the calcium phosphate-based biominerals has been an issue of debate, where the early literature found evidence of an amorphous precursor in bone [1, 10] and turkey tendons [11]. This concept has been revived in recent reports [12], and verified when an amorphous calcium phosphate (ACP) precursor was demonstrated in zebrafish fin bones

lgowe@mse.ufl.edu.

[13], where granular ACP particles crystallize into platelets of hydroxyapatite. Such transformations might also include an intermediate phase, such as octacalcium phosphate, as has been described for bone formation [14].

Using an *in-vitro* model system, we and other labs have studied and utilized a polymer-induced amorphous precursor [15] as a transient (but necessary) phase to form calcium carbonate [16-21] and calcium phosphate [12, 22] structures that have striking resemblance, in morphology and crystallographic makeup, to those found in nature. Here, we report the formation of multi-laminated calcium phosphate spherules, synthesized from a polymer-induced liquid-precursor, or PILP phase, which appear similar to those observed in the calcium phosphate deposits in the basement membrane of the thin loop of Henle in the kidneys [23]. These multi-layered biominerals, also known as Randall's plaques, consist of alternating strata of organic- and inorganic-dense materials [24] that are believed to serve as attachment sites for calcium oxalate overgrowths to form into kidney stones [25-27]. Although the synthesis of the laminated spherules (or spherulites) of calcium phosphate has been previously reported before by Bigi, et al. [28], the reference to the formation of these spherulitic structures from an amorphous precursor is not discussed. A deeper understanding of the formation of these spherules using this *in-vitro* model system may provide important information to the mechanisms involved in pathological biomineralization.

EXPERIMENTAL SECTION

Materials

Sodium bicarbonate ($NaHCO_3$), calcium acetate monohydrate ($Ca(CH_3COO)_2{\cdot}H_2O$), sodium phosphate monobasic ($NaH_2PO_4{\cdot}H_2O$), sodium chloride (NaCl) were purchased from Fisher. Poly-L-aspartic acid (MW_{vis} 10300) was bought from Sigma. An anionic phosphorylated peptide, $[DEPs]_6D$, was synthesized via a solid phase Fmoc chemistry [29]. High purity 18.2-MΩ deionized water was used for all solutions.

Calcium Phosphate Mineralization

Separate stock solutions of 12 mM $Ca(CH_3COO)_2{\cdot}H_2O$ and 12 mM $NaH_2PO_4{\cdot}H_2O$ were prepared. The ionic strength of each solution was maintained at 36 mM using NaCl. The pH was set to 6 using dilute HCl or NaOH. Equal volumes of the solutions were mixed by slow drop-wise addition of the phosphate-containing solution to the Ca^{2+}-solution at 80 °C. Prior to the addition, different amounts of poly-L-aspartic acid were added to the Ca^{2+}-containing solution. The total volume of the mixture was ~25 mL. There was no mechanical stirring during precipitation.

Structural Characterization

Scanning electron micrographs were taken using a JEOL 6400 scanning electron microscope. For the as-synthesized samples, the precipitates were mounted on aluminum stubs and coated with gold. Some precipitates were coated with carbon and platinum and then sequentially milled with a Focused Ion-beam Dual-beam Strata DB235 to view the cross-section of the spherules. Polarized optical microscopy with a first-order red λ-plate was performed using an Olympus BX-60 optical microscope equipped with an MTI 3CCD camera.

For x-ray diffraction analysis, the precipitates were filtered through a 0.22-μm pore size filter (Millipore) and subsequently washed with water. The precipitates were then air-dried and immediately characterized using a Philips APD 3720 x-ray diffractometer with CuKα radiation, using a step size of 0.01° with a time of 2 s/step. Quantification of the crystalline

calcium phosphate present in the precipitates was done using the Rietveld method (see supporting information).

RESULTS AND DISCUSSION

Calcium Phosphate Polymorphs

The polymorph of the calcium phosphate phases formed at different concentrations of the anionic poly-L-aspartic acid (PD) is presented in the XRD data in Figure 1. The precipitates that were synthesized in the absence of the organic additive can be indexed to hydroxyapatite, HA (ICSD 09-432), with the main peak centered at 31.8° (2θ). An increase in the concentration of the PD during the synthesis resulted in a simultaneous increase in the formation of octacalcium phosphate, OCP (ICSD 26-1056), and a decrease in the HA phase. This is clearly seen in the enhancement of the 4.7° (2θ) peak associated with OCP and the decline of the 31.8° (2θ) peak associated with HA. Rietveld analysis of the XRD data in Figure 1 was performed to determine the relative compositions of these crystalline phases as a function of the polypeptide additive (Figure 2). In the absence of PD, 100% HA (0% OCP) was observed. This decreased to ~76% HA (24% OCP) as the PD was increased to 50 μg/mL. Not only was the relative composition of the crystalline calcium phosphate varied with increasing PD, the occurrence of an amorphous calcium phosphate (ACP) phase became more prevalent, as manifested in the increase of the broad peak at ~18° (2θ) in the XRD data (arrow in Figure 1). It has to be pointed out that the XRD sample preparation was consistent in all of the runs, making sure that an appropriate amount of the synthesized calcium phosphate was packed on the glass sample holder to eliminate possible x-ray interaction from the amorphous substrate of the sample holder.

Polymer Effect on the Spherule Morphology

Micrographs of the synthesized calcium phosphate as a function of PD concentration are presented in Figure 3. For samples grown in 10 – 50 μg/mL PD, the precipitates were polycrystalline with spherulitic morphology, as evidenced by the Maltese-cross extinction patterns under cross-polarized light (Figures 3b-d). A gypsum λ-plate was used in order to examine both amorphous and crystalline materials. Isotropic material will appear magenta in color, so the cross is less pronounced, but the orange and blue quadrants are characteristic of the spherulitic structure as well. A schematic representation of the Maltese cross for one of the calcium phosphate spherules is depicted in the inset in Figure 3c. The dimensions of the particles were often larger than 20 μm, which can be seen in the scanning electron micrographs (Figure 3f-h). The samples synthesized without PD, which grow no larger than 10 μm (Figures 3a, e), did not distinctively exhibit a Maltese cross because they were rough and exhibited a brown/black color under the polarized light (Figure 3a) that made it difficult to observe an extinction cross. However, upon a digital magnification of one of the larger particles, a very faint extinction cross is observed (inset, Figure 3a), indicating the polycrystallinity and spherulitic nature of the samples.

The spherulites formed at larger amounts of PD (20-50 μg/mL) were less spherical and had a tendency to form film-like precipitates. These flattened spherules may be due to the deposition of the PILP droplets at the bottom of the crystallization dish (Figure 3f), as has been observed in the $CaCO_3$ PILP system. Note that during the synthesis of the precipitates, no stirring was performed, which allowed for settling of the precipitates; stirring likely would have led to more spherical 3-dimensional precipitates. There were some samples, particularly those synthesized at 50 μg/mL PD, where non- or weakly birefringent films were starting to transform into highly birefringent samples (Figure 3d and Supporting Figure 1). This is attributed to the crystallization of the amorphous calcium phosphate precursor, which was observed via XRD to be abundant at high concentrations of PD.

"Molten" Spherules

A close inspection of the calcium phosphate samples grown at 20-50 μg/mL PD concentration shows concentric laminations and tangential striations (Figure 4). The peculiar precipitate in Figure 4b appears to have developed from the flow of a liquid-like precursor. Such "molten" structures are not observed at low concentrations of PD (0 – 10 μg/mL), suggesting that the liquid-like precursor is induced or stabilized more effectively at higher PD concentrations.

The evolution of the molten spherulite structure is demonstrated in Figure 5, where the precipitates were extracted from the crystallization solution at different reaction times. Within 5 minutes of reaction, small non-faceted liquid-like ACP precipitates (depicted by the arrow in Figure 5a) start to coalesce to form larger structures. A similar agglomeration process has been observed in the formation of spherulites of vaterite in the $CaCO_3$ system [30]. At this point, the structures are non-birefringent, and do not exhibit any lamination or striation. The samples taken out after 15 minutes of precipitation are larger, birefringent and striated, with an appearance of having "flowed" during the crystallization process (Figure 5b). Note that the samples contain regions with smooth and rough textures. Samples that were taken after 30 minutes of the reaction typically exhibited rougher texture and more distinct polycrystalline grains (Figure 5c) as they became crystalline.

The formation of layered textures in the spherules is believed to be caused by the incorporation of the polymer within the structures. The initial amorphous liquid-like precursor contains a high concentration of the polypeptide additive [31]. As this molten structure transforms into its stable crystalline state, the organic additive is excluded, but some of it becomes entrapped due to transport limitations within the solidifying amorphous phase, thus generating concentric laminations and striations. The exclusion of polymer in diffusion-limited periodic zones has been directly observed in the $CaCO_3$ films formed by a PILP phase using fluorescently labeled PD [32]. Unfortunately, the samples here were too thick to distinguish any difference in the amount of polypeptide within the different zones due to the complexity of these three-dimensional globular samples; but the more porous layers likely result from the enrichment of polymer and water in those zones.

The exclusion of the polymer during the transformation of the amorphous phase also results in the roughening of the precipitates, which occurs from the core to the periphery of the spherules. This is seen in the progressive cross-sectional analysis of a spherulite shown in Figure 6, where two smooth regions are highlighted. Notice that the sliced sections of the spherule show that the smooth region is observed at the periphery while the coarse region is observed at the core (Figure 6b, c). The roughening of the spherule may not encompass the whole particle, as smooth regions may remain at the outer layer of the sample, perhaps protected by an accumulation of polymer, as has been observed for $CaCO_3$ spherules [32].

Spherules using Synthetic Peptides

Utilizing the same crystallization technique, an anionic phosphorylated peptide with a sequence of $[DEPs]_6D$, was used instead of PD, where D denotes aspartic acid, E glutamic acid, and Ps phosphoserine. This peptide is a mimic of the phosphorylated sequence in some proteins that are thought to be important in the calcium phosphate-based biomineral formation [33, 34]. Similar to the effect of PD on the development of the spherules, at low concentration of the peptide (10 μg/mL), spherical precipitates were formed (Figure 7a, d), while at high concentrations (20-50 μg/mL), large molten spherulitic structures were produced (Figure 7b-c, e-f). Also, weakly birefringent films observed under polarized light were stabilized at high concentrations of the peptide (Figure 7b-c).

Implication to Randall's plaque and kidney stone formation

The ability to mimic various biomineral features via a polymer-induced liquid-like precursor has been extensively explored with calcium carbonate and calcium phosphate biominerals [12, 15-22, 35]. The polymer plays an important role in stabilizing the amorphous precursor, which can either undergo a dissolution-recrystallization event into the more stable equilibrium morphology [30, 36] or undergo a pseudomorphic transformation [15], where the waters of hydration and organic additives are driven out while maintaining the over-all morphology of the precursor. Based on the micrographs presented in this paper, it is likely that the formation of the multi-laminated calcium phosphate spherules occurs primarily via the latter crystallization route, where the structures formed seemed to solidify and crystallize from the amorphous precursor (although there appears to be partial recrystallization, which forms the conventional platy habit of the polycrystals). The transformation appears to proceed from the core to the periphery of the spherules, thereby roughening the precipitates from the inside out. The exclusion of the organic additive is transport-limited, which entraps the organic additive within concentric layers of the spherules.

Due to the similarity of the synthetic spherules presented here to the multi-lamellar structures of the Randall's plaque, we suggest that the formation of these pathological deposits may occur via a polymer-induced liquid-precursor phase *in vivo*. There are many anionic proteins in the urinary environment that might be able to induce such an amorphous phase, such as osteopontin for example, which is observed in close association with the crystals of Randall's plaque [24, 37]. With the abundance of other organic molecules present in urine, e.g. proteins, lipids and carbohydrates [38-40], which may be adventitiously adsorbed and then excluded to form lamellae during the pseudomorphic transformation of the biomineral, a multi-lamellar spherule structure with alternating organic- and crystal-dense layers may be formed, as observed in the electron micrographs of these plaques [24, 25]. The inability to observe the organic-rich layer in our biomimetic spherules is because of the relatively low concentration of additive present in our crystallization medium (only micromolar quantities were used to induce the PILP process). In the urinary environment, organic materials could feasibly reside in these organic-enriched zones if the crystallization proceeded via an amorphous precursor. Because of the natural radial growth pattern found in spherulites, the crystallites within the structures are typically oriented at 90° with respect to the concentric lamellae. This morphological feature may have been misinterpreted as an "epitaxial" relationship between the organic-rich lamellae and the inorganic crystallites in the Randall's plaque [38, 41], especially when there is a seemingly perpendicular relationship between these two alternating layers. However, this apparent epitaxy is incidental, as the crystallites within spherules would be radial in their growth regardless of an existing organic lamella. In other words, these multi-laminated structures may not arise from episodic deposition of mineral and organics, but from one initially formed globule that subsequently breaks down into layers as it crystallizes.

Although it has been observed that the final crystallographic phase of the Randall's plaque is apatite, it is not certain as to what mineral stage of the spherule, e.g. ACP, OCP or HA, effectively serves as the substrate for the subsequent calcium oxalate mineralization. Studies are currently under way in our lab to answer this fundamental question by utilizing the molten calcium phosphate structures as substrates for calcium oxalate overgrowth, as we strive to develop a model system of the core-shell calcium phosphate-calcium oxalate urinary stones.

Supplementary Material

Refer to Web version on PubMed Central for supplementary material.

Acknowledgments

This work was supported by the National Institutes of Health as a Bioengineering Research Partnership (BRP) Grant RO1 DK59765.

REFERENCES

1. Termine JD, Posner AS. Infrared analysis of rat bone-Age dependency of amorphous and crystalline mineral fractions. Science. 1966; 153:1523. &. [PubMed: 5917783]
2. Posner AS. Crystal chemistry of bone mineral. Physiol Rev. 1969; 49:760. &. [PubMed: 4898602]
3. Mann S. Mineralization in biological systems. Struct Bond. 1983; 54:125–174.
4. Lowenstam HA, Weiner S. Transformation of amorphous calcium phosphate to crystalline dahllite in the radular teeth of chitons. Science. 1985; 227:51–53. [PubMed: 17810022]
5. Taylor MG, Simkiss K, Greaves GN, Okazaki M, Mann S. An x-ray absorption spectroscopy study of the structure and transformation of amorphous calcium carbonate from plant cystoliths. Proc R Soc London, Ser B. 1993; 252:75–80.
6. Beniash E, Aizenberg J, Addadi L, Weiner S. Amorphous calcium carbonate transforms into calcite during sea urchin larval spicule growth. Proc R Soc London, Ser B. 1997; 264:461–465.
7. Weiss IM, Tuross N, Addadi L, Weiner S. Mollusc larval shell formation: Amorphous calcium carbonate is a precursor phase for aragonite. J Exp Zool. 2002; 293:478–491. [PubMed: 12486808]
8. Raz S, Hamilton PC, Wilt FH, Weiner S, Addadi L. The transient phase of amorphous calcium carbonate in sea urchin larval spicules: The involvement of proteins and magnesium ions in its formation and stabilization. Adv Funct Mater. 2003; 13:480–486.
9. Weiner S, Sagi I, Addadi L. Choosing the crystallization path less traveled. Science. 2005; 309:1027–1028. [PubMed: 16099970]
10. Posner AS, Betts F. Synthetic amorphous calcium phosphate and its relation to bone-mineral structure. Acc Chem Res. 1975; 8:273–281.
11. Eanes ED, Lundy DR, Martin GN. X-Ray diffraction study of mineralization of turkey leg tendon. Calcif Tissue Res. 1970; 6:239. &. [PubMed: 5500677]
12. Olszta MJ, Cheng XG, Jee SS, et al. Bone structure and formation: A new perspective. Mater Sci Eng, R. 2007; 58:77–116.
13. Mahamid J, Sharir A, Addadi L, Weiner S. Amorphous calcium phosphate is a major component of the forming fin bones of zebrafish: Indications for an amorphous precursor phase. Proc Natl Acad Sci USA. 2008; 105:12748–12753. [PubMed: 18753619]
14. Crane NJ, Popescu V, Morris MD, Steenhuis P, Ignelzi MA. Raman spectroscopic evidence for octacalcium phosphate and other transient mineral species deposited during intramembranous mineralization. Bone. 2006; 39:434–442. [PubMed: 16627026]
15. Gower LB, Odom DJ. Deposition of calcium carbonate films by a polymer-induced liquid-precursor (PILP) process. J Cryst Growth. 2000; 210:719–734.
16. Xu GF, Yao N, Aksay IA, Groves JT. Biomimetic synthesis of macroscopic-scale calcium carbonate thin films. Evidence for a multistep assembly process. J Am Chem Soc. 1998; 120:11977–11985.
17. Gower LA, Tirrell DA. Calcium carbonate films and helices grown in solutions of poly(aspartate). J Cryst Growth. 1998; 191:153–160.
18. Olszta MJ, Gajjeraman S, Kaufman M, Gower LB. Nanofibrous calcite synthesized via a solution-precursor-solid mechanism. Chem Mater. 2004; 16:2355–2362.
19. Gehrke N, Nassif N, Pinna N, Antonietti M, Gupta HS, Colfen H. Retrosynthesis of nacre via amorphous precursor particles. Chem Mater. 2005; 17:6514–6516.
20. Cheng XG, Gower LB. Molding mineral within microporous hydrogels by a polymer-induced liquid-precursor (PILP) process. Biotechnol Prog. 2006; 22:141–149. [PubMed: 16454504]
21. Amos FF, Sharbaugh DM, Talham DR, Gower LB, Fricke M, Volkmer D. Formation of single-crystalline aragonite tablets. Langmuir. 2007; 23:1988–1994. [PubMed: 17279685]
22. Amos, FF.; Olszta, MJ.; Khan, SR.; Gower, LB. Relevance of a polymer-induced liquidprecursor (PILP) mineralization process to normal and pathological biomineralization. In: Königsberger, E.;

Königsberger, L., editors. Medical aspects of solubility. John Wiley & Sons, Ltd.; West Sussex, England: 2006. p. 125-217.

23. Evan AP, Lingeman JE, Coe FL, et al. Randall's plaque of patients with nephrolithiasis begins in basement membranes of thin loops of Henle. J Clin Invest. 2003; 111:607–616. [PubMed: 12618515]
24. Evan AP, Coe FL, Rittling SR, et al. Apatite plaque particles in inner medulla of kidneys of calcium oxalate stone formers: Osteopontin localization. Kidney Int. 2005; 68:145–154. [PubMed: 15954903]
25. Randall A. The origin and growth of renal calculi. Ann Surg. 1937; 105:1009–1027. [PubMed: 17856988]
26. Low RK, Stoller ML. Endoscopic mapping of renal papillae for Randall's plaques in patients with urinary stone disease. J Urol. 1997; 158:2062–2064. [PubMed: 9366312]
27. Khan SR. Calcium phosphate calcium oxalate crystal association in urinary stones: Implications for heterogeneous nucleation of calcium oxalate. J Urol. 1997; 157:376–383. [PubMed: 8976301]
28. Bigi A, Boanini E, Walsh D, Mann S. Morphosynthesis of octacalcium phosphate hollow microspheres by polyelectrolyte-mediated crystallization. Angew Chem Int Ed. 2002; 41:2163–2166.
29. Dai, L. Mechanistic study of the polymer-induced liquid-precursor (PILP) process: Relevance to biomineralization. University of Florida; Gainesville, Florida: 2006.
30. Rieger J, Frechen T, Cox G, Heckmann W, Schmidt C, Thieme J. Precursor structures in the crystallization. Faraday Discuss. 2007; 136:265–277. [PubMed: 17955814]
31. Dai L, Douglas EP, Gower LB. Compositional analysis of a polymer-induced liquid-precursor (PILP) amorphous CaCO3. J Non Cryst Solids. 2008; 354:1845–54.
32. Dai L, Cheng X, Gower LB. Transition bars during transformation of an amorphous calcium carbonate precursor. Chem Mater ASAP. 2008 DOI: 10.1021/cm800760p.
33. Veis A. Mineral matrix interactions in bone and dentin. J Bone Miner Res. 1993; 8:S493–S497. [PubMed: 8122518]
34. Termine JD, Kleinman HK, Whitson SW, Conn KM, Mcgarvey ML, Martin GR. Osteonectin, a bone-specific protein linking mineral to collagen. Cell. 1981; 26:99–105. [PubMed: 7034958]
35. Gower LB. Biomimetic model systems for investigating the amorphous precursor pathway and its role in biomineralization. Chem Rev. 2008 in press.
36. Eanes ED, Posner AS. Intermediate phases in basic solution preparation of alkaline earth phosphates. Calcif Tissue Res. 1968; 2:38. &. [PubMed: 5674914]
37. Atmani F, Glenton PA, Khan SR. Identification of proteins extracted from calcium oxalate and calcium phosphate crystals induced in the urine of healthy and stone forming subjects. Urol Res. 1998; 26:201–207. [PubMed: 9694603]
38. Boyce WH. Organic matrix of human urinary concretions. Am J Med. 1968; 45:673. &. [PubMed: 5687257]
39. Nishio S, Abe Y, Wakatsuki A, et al. Matrix glycosaminoglycan in urinary stones. J Urol. 1985; 134:503–505. [PubMed: 4032548]
40. Khan SR, Atmani F, Glenton P, Hou ZC, Talham DR, Khurshid M. Lipids and membranes in the organic matrix of urinary calcific crystals and stones. Calcif Tissue Int. 1996; 59:357–365. [PubMed: 8849402]
41. Carr JA. The pathology of urinary calculi: radial striation. Br J Urol. 1953; 25:26–32. [PubMed: 13032398]

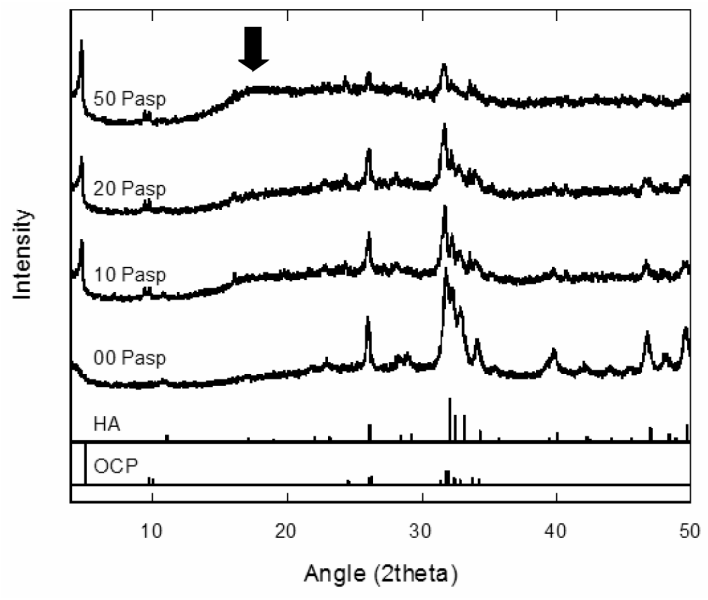

Figure 1.
X-ray diffraction of calcium phosphate spherules grown at different concentrations of PD. The arrow points to the broad peak associated with the stabilization of ACP at 50 μg/mL PD. Peaks are indexed to HA (ICSD 09-432) and OCP (ICSD 26-1056).

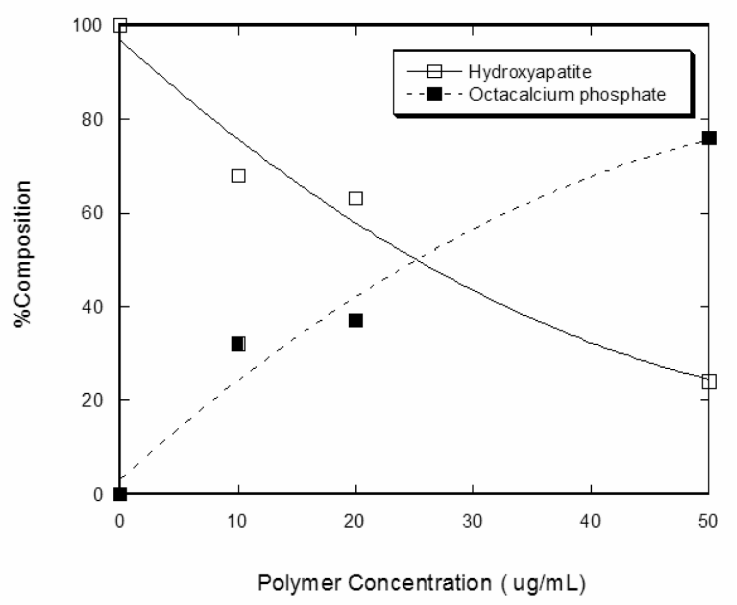

Figure 2.
Relative composition of the crystalline calcium phosphate polymorphs (HA and OCP) evaluated via the Rietveld method.

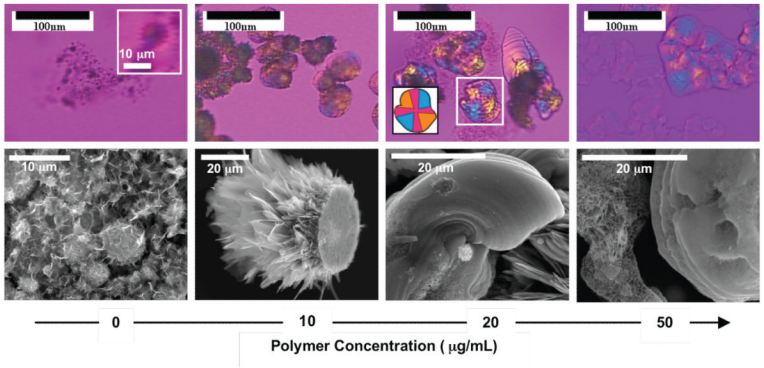

Figure 3.

(a-d) Polarized optical and (e-h) scanning electron micrographs of the calcium phosphate spherules grown at different concentrations of the polypeptide. Inset in (a) shows a digital magnification of a relatively large calcium phosphate spherule showing the extinction cross. Inset in (c) shows a schematic representation of the highlighted spherule showing how the Maltese cross appears for polycrystalline spherulites examined with a gypsum λ-plate.

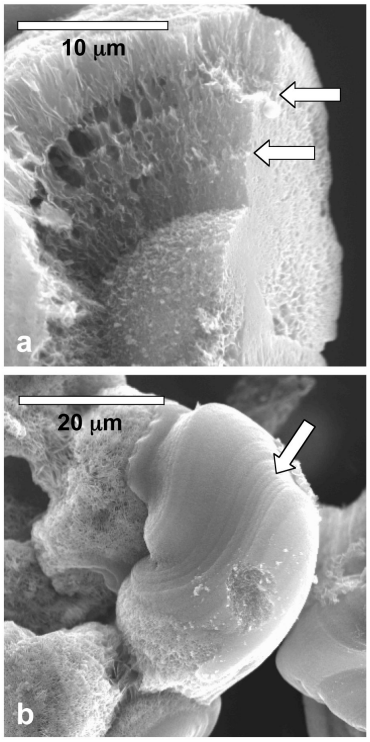

Figure 4.
Scanning electron micrographs of the calcium phosphate spherules, where the arrows point to the (a) concentric laminations and (b) tangential striations within the structures. The samples were grown in the presence of 50 μg/mL PD.

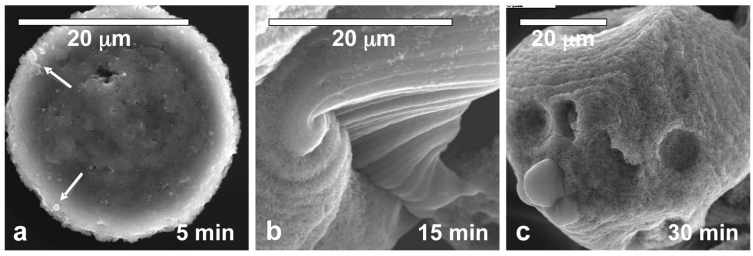

Figure 5.

Evolution of the calcium phosphate spherules formed at high concentration of PD (50 μg/mL) at different reactions times: (a) 5 min, (b) 15 min and (c) 30 min. Arrows in (a) point to the ACP precursor droplets that coalesced into a larger structure. A roughening of the texture within the molten spherulite was observed over time.

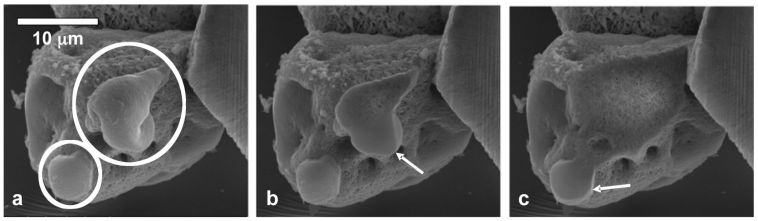

Figure 6.
Scanning electron micrographs (a) before and (b, c) after progressive FIB cross-sectional slicing of the calcium phosphate spherules. The smooth regions reside mainly at the periphery of the spherules.

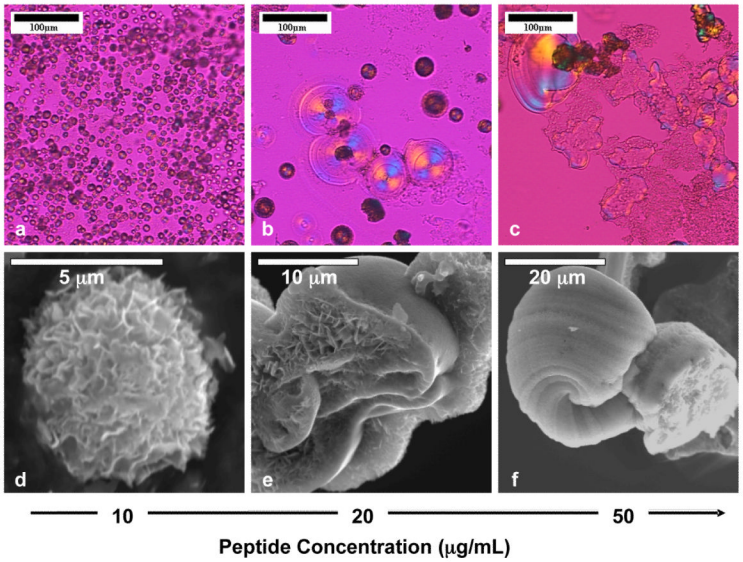

Figure 7.
Calcium phosphate spherules formed in the presence of various concentrations of the biomimetic phosphorylated peptide, [DEPs]6D.